Computational study of Al droplet combustion in a burning solid propellant environment

Muller Mathieu, Davidenko Dmitry, Giovangigli Vincent

DOI: 10.13009/EUCASS2019-202

Computational study of Al droplet combustion in a burning solid propellant environment

Muller Mathieu[1], Davidenko Dmitry[1], Giovangigli Vincent[2]
[1]*ONERA, Chemin de la Hunière, 91123 Palaiseau, France*
[2]*Ecole Polytechnique, 91128, Palaiseau, France*

Abstract

Combustion of a single aluminum particle in a solid propellant flame is studied with complex chemistry and detailed molecular transport. The reacting flow around the droplet is treated as spherically symmetric. In a new droplet model, an average effect of the alumina cap is taken into account. The combustion model is validated with respect to experimental results and an axisymmetric simulation. The combustion of two particle classes is simulated with different surface reaction mechanisms. The effect of surface mechanism on the temporal evolution of particle parameters is investigated. The burning time and residue size are evaluated for the simulated cases.

Keywords: Aluminum droplet, combustion modeling, detailed chemical kinetics, surface reactions, numerical simulation, burning time, combustion residue

1. Introduction

Combustion of metals provides an important energy release and is widely used for propulsion purposes. In particular, aluminum particles are often introduced as an energetic component in solid propellant formulations to improve the specific impulse of solid rocket motors. Metal particles burn in a gaseous flow and produce condensed-phase residues. This process need to be properly characterized in order to predict possible negative effects, for example thrust losses due to the condensed phase. Detailed modeling of individual particle combustion can provide such a characterization but it is a challenging problem because it needs to take into account complex physico-chemical phenomena.

In combustion simulations, a modeling methodology based on solving the Navier-Stokes equations for an axisymmetric steady-state reacting flow around an aluminum droplet has been actively used since the 2000s. The evolution of the modeling approach can be seen from particular publications. A complete combustion model of an aluminum droplet in an oxygen-containing atmosphere was presented by Beckstead et al. [1] describing principal physico-chemical processes. Gas-phase and heterogeneous chemistry was represented by several global reactions. An expression for the rate of alumina condensation was derived from the nucleation theory. This modeling approach was later improved by Washburn et al. [2] by replacing the global gas-phase reactions with a detailed kinetic mechanism developed by Catoire and Swihart. However, only Al evaporation was modeled by assuming the equilibrium vapor fraction at the droplet surface.

A detailed kinetic mechanism for the aluminum surface was recently developed by Glorian [3][4]. This surface mechanism together with the detailed gas-phase mechanism by Catoire and Swihart was used by Glorian et al. [5] for simulations of the aluminum droplet combustion in different oxidizers with the CPS code developed at AGS. A 2D axisymmetric flow of a multispecies reacting gas was simulated around a constant-diameter aluminum droplet without oxide cap. Two global irreversible reactions converting the gas-phase alumina into the liquid phase were added to the gas-phase kinetics.

At ONERA, numerical simulations of the aluminum droplet combustion in the 2D axisymmetric approach were performed by Orlandi in the early 2000s using the MSD code. In these simulations different gas-phase kinetic mechanisms were used first for the combustion in air [6] and then in the hot gases from a burning solid propellant [7]. Later simulations of the aluminum droplet combustion for some particular conditions were performed using a similar approach with the CEDRE code.

This short overview shows that the common practice consists in simulating a reacting flow around a constant-diameter spherical droplet in the 2D axisymmetric configuration. Alternatively, a 1D spherically-symmetric approach was proposed by Cho et al. [8] for the droplet combustion with detailed models for the

DOI: 10.13009/EUCASS2019-202

chemical kinetics and molecular transport. A numerical model based on this 1D approach was used by Bucher et al. [9] to model the aluminum droplet combustion by assuming partial equilibrium for the gaseous species. Recently, Savel'ev et al. [10] developed a model of alumina condensation by nucleation of $(Al_2O_3)_n$ clusters together with a 1D quasi-steady approach for the reacting flow.

The experimental results of Bucher et al. [9] have been actively used for validation of simulation results. New experimental results on the aluminum particle combustion in hot gases from an AP/HTPB propellant are now available from the work of Chen et al. [11], in particular temperature profiles in the flame around a particle measured by the two-color imaging calorimetry. PLIF technique for Al atoms have been recently developed and used at ONERA [12][13] to study the aluminum combustion in solid propellant flames.

A 1D unsteady combustion model was recently developed at ONERA to simulate the aluminum droplet combustion with detailed models for the chemical kinetics and molecular transport. This model is an improvement of the one, which was used previously to study the aluminum droplet combustion in the O_2/Ar, CO_2, and H_2O oxidizers [14]. The first purpose of this paper is to describe the new modeling approach and to demonstrate validation results. The second purpose is to present a study of the aluminum particle combustion under conditions of a burning solid propellant and to show the importance of the reaction mechanism for the surface kinetics.

2. A new 1D combustion model of an aluminum droplet with a cap

The new modeling approach presented below is based on several models in relation with the droplet and the reactive gas. The aluminum droplet may have a cap of aluminum oxide and other bulk materials. A droplet with a cap will be called together a particle. For the 1D approach, both the particle and the flow are assumed to be spherically symmetric. The cap cannot fit this assumption however its average effect can be taken into account.
In the previous work [14], the 1D approach was based on the quasi-steady-state assumption, which implies that the gas flow state adapts instantly to any change in the particle state during the combustion process. The new 1D approach allows simulating the temporal evolution of the particle and gas flow.

2.1 Thermodynamic model

The particle and gas flow are considered as multicomponent or multispecies. The components are grouped in three phases: gaseous, surface and bulk. The particle is composed of bulk species (inner part) and surface species (interface with the gas).

Thermodynamic properties of any species k are defined by its molar mass W_k, temperature-dependent heat capacity in mass units $c_{Pk}(T)$, standard enthalpy $h_k(T^o)$, and entropy $s_k(P^o, T^o)$. All these data are obtained from thermodynamic databases.

The gaseous phase obeys the equation of state for an ideal gas. For the bulk components, the density is temperature-dependent. Solidification is not actually taken into account for the bulk components.

2.3 Particle model

A simple geometrical representation is adopted for the particle as shown in Figure 1. The droplet and its cap are spherical segments of the same radius r_p. The cap is defined geometrically by its thickness h_{cap}. The area of the particle surface A_p is decomposed into two parts corresponding to the aluminum A_{alu} and the cap A_{cap}.

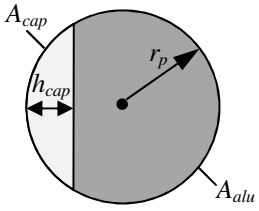

Figure 1 – Geometrical representation of an aluminum droplet with a cap.

Knowing the relative thickness of the cap h_{cap}/r_p, it is easy to calculate the relative area and volume of the aluminum droplet:

DOI: 10.13009/EUCASS2019-202

$$\frac{A_{alu}}{A_p} = 1 - \frac{1}{2}\frac{h_{cap}}{r_p} \tag{1}$$

$$\frac{V_{alu}}{V_p} = 1 - \frac{1}{4}\left(\frac{h_{cap}}{r_p}\right)^2\left(3 - \frac{h_{cap}}{r_p}\right) \tag{2}$$

By introducing the mass fraction of aluminum $Y_{alu} = m_{alu}/m_p = m_{alu}/(m_{alu}+m_{cap})$, the following relation may be written for the relative volume:

$$\frac{V_{alu}}{V_p} = \frac{m_{alu}}{m_p}\frac{\rho_p}{\rho_{alu}} = Y_{alu}\left(Y_{alu} + (1 - Y_{alu})\frac{\rho_{alu}}{\rho_{cap}}\right)^{-1} \tag{3}$$

where ρ is the bulk density.

In the present modeling approach, the heat transfer within the particle is neglected by assuming its temperature to be homogeneous hence the particle thermal state is defined by a single temperature T_p. For a given set of parameters m_{alu}, m_{cap}, and T_p, the particle geometry can be determined using the above equations.
It is also assumed that the cap material is produced by heterogeneous reactions on the open surface of the aluminum droplet and this material is instantly absorbed by the cap. This means that the open surface of the droplet is considered always free from bulk species. The cap surface has no mass exchange with the surrounding gas.

The evolution of the particle state is governed by the following differential equations for the component masses and the particle enthalpy:

$$\frac{\mathrm{d}m_k}{\mathrm{d}t} = A_{alu}\dot{s}_k + \dot{m}_{b,k} \tag{4}$$

$$\frac{\mathrm{d}(m_p h_p)}{\mathrm{d}t} = A_{alu}\sum_{k=k_B}^{K_B}\dot{s}_k h_k + \dot{m}_b h_b + Q_p \tag{5}$$

where $\dot{s}_k$ is the net production rate of the k^{th} bulk species per unit surface due to heterogeneous reactions; $\dot{m}_{b,k}$ and $\dot{m}_b h_b$ are the boiling terms; Q_p is the rate of heat exchange with the exterior; k_B and K_B are the indices of the first and last bulk species respectively. The cap mass m_{cap} is the sum of the bulk components excepting the bulk aluminum.

Aluminum is the only component for which the boiling condition is introduced in the present model. If the particle temperature T_p is below the boiling point T_b, the boiling terms $\dot{m}_{b,k}$ and $\dot{m}_b h_b$ are zero. For the boiling regime, the condition of constant temperature $T_p = T_b$ is used instead of the energy equation (5). T_b is found by solving the following nonlinear equation, which expresses the equality between the ambient pressure P and the pressure of saturated aluminum vapor on the right-hand side:

$$P = P^\circ \exp\left(\left[s^\circ_{\mathrm{Al(G)},b} - s^\circ_{\mathrm{Al(B)},b} - \left(h_{\mathrm{Al(G)},b} - h_{\mathrm{Al(B)},b}\right)/T_b\right] W_{\mathrm{Al}}/R\right) \tag{6}$$

where indices Al(B) and Al(G) denote the aluminum in the bulk (liquid) and gas phases respectively; s° is the entropy at standard pressure P°; R is the universal gas constant.

The condition of constant temperature $T_p = T_b$ implies that the boiling heat rate compensates the particle heating from the exterior:

$$\dot{m}_{b,\mathrm{Al(B)}}\left(h_{\mathrm{Al(G)},b} - h_{\mathrm{Al(B)},b}\right) = -Q_p \tag{7}$$

Due to the sign convention, the particle is heated if $Q_p > 0$. This last equation is used to determine the $\dot{m}_{b,k}$ term in equation (4) for the Al(B) component.

The initial conditions for the particle state can be defined by specifying the particle diameter $D_0 = 2r_{p,0}$, temperature $T_{p,0}$, and the aluminum mass fraction $Y_{alu,0}$. With the steady-state assumption, D and Y_{alu} remain constant whereas T_p is determined to verify the boundary conditions for the gas flow on the particle surface, which pertain to the surface model.

2.4 Gas flow model

Two simplifying assumptions are adopted for the gas flow model: (i) no radiative heat transfer; (ii) liquid alumina Al_2O_3(L) generated by the gas-phase reactions is treated as a gas species in the equation of state and the molecular transport model thus assuming infinitely fine smoke particles.

DOI: 10.13009/EUCASS2019-202

The governing equations describing an unsteady spherically-symmetric isobaric flow of reacting gas around a particle are:

$$\frac{\partial(A\rho)}{\partial t} + \frac{\partial M}{\partial r} = 0 \tag{8}$$

$$\frac{\partial(A\rho h)}{\partial t} + \frac{\partial(Mh + Aq)}{\partial r} = 0 \tag{9}$$

$$\frac{\partial(A\rho Y_k)}{\partial t} + \frac{\partial(MY_k + A\,J_k)}{\partial r} = A\,\dot{m}_k \tag{10}$$

with $A = 4\,\pi\,r^2$, the spherical surface area corresponding to radial coordinate r; ρ, the gas density determined from the ideal gas law for a given ambient pressure; $M = A\rho u$, the mass flow rate; h, the gas enthalpy equal to the sum of $Y_k\,h_k$ of all the gaseous species; q, the heat flux and J_k, the diffusion mass flux of the k^{th} gas species defined by the molecular transport model; $\dot{m}_k$, the net production rate per unit volume of the k^{th} gas species defined by the gas-phase chemical kinetics.

The chemical kinetic model for the gas is based on the mechanism of Catoire and Swihart [2][5], which was enhanced with 2 reactions for thermal NO and 7 reactions for HCO from the GRI-Mech 3.0 mechanism.

In the gas-phase kinetic model of Glorian et al. [5], there are two global reactions producing liquid alumina Al_2O_3(L) from gas-phase isomers Al_2O_3 and Al_2O_{3c}:

$$Al_2O_3 \Rightarrow Al_2O_3(L),\ \ Al_2O_{3c} \Rightarrow Al_2O_3(L) \tag{11}$$

In the present model, these reactions are written in the reversible form to allow dissociation of Al_2O_3(L) and to prevent from excessive temperature increase in the flame:

$$Al_2O_3 \Leftrightarrow Al_2O_3(L),\ \ Al_2O_{3c} \Leftrightarrow Al_2O_3(L) \tag{12}$$

It should be noted that the rate constants used for these reactions are very high and do not limit the production of Al_2O_3(L).

The molecular transport model uses full multicomponent formalism with the Soret and Dufour effects due to thermodiffusion. The diffusion velocity of the k^{th} gas species is defined as:

$$v_k = -\sum_{j=k_G}^{K_G} D_{kj}\left(\nabla X_j + \chi_j \nabla \ln T\right) \tag{13}$$

with k_G and K_G, the indices of the first and last gas species respectively; D_{kj}, the element of the diffusion matrix corresponding to species k and j; ∇X_j, the mole fraction gradient of the j^{th} species; χ_j, the thermal diffusion ratio of the j^{th} species.

The expressions for the molecular fluxes are:

$$J_k = -\rho Y_k v_k \tag{14}$$

$$q = -\lambda \nabla T + \sum_{k=k_G}^{K_G} (h_k J_k + P\chi_k v_k) \tag{15}$$

λ is the thermal conductivity of the gas mixture.

Transport coefficients λ, D_{kj}, and χ_k are determined by approximate methods developed by Ern and Giovangigli [15][16] and implemented in the EGlib library. EGlib uses the transport properties of individual species and the binary diffusion coefficients, which are calculated from molecular parameters and approximated by temperature polynomials with the help of the TRANFIT utility from the CHEMKIN-II library.

2.4 Particle surface model

The particle surface is a physical boundary between the particle interior and the gas flow as well as an interface between the corresponding models. At the open surface of the aluminum droplet, heterogeneous reactions take place between species from the three phases. The rates of species production by the heterogeneous reactions are determined using the chemical kinetic mechanism from [5] and according to the same formalism as in the CHEMKIN library.

Surface species represent a particular phase, which separates the bulk species on the particle side and

DOI: 10.13009/EUCASS2019-202

the gas species on the flow side. Their quantities can be characterized by the surface site fractions Z_k and by the surface site densities γ_k, which are related as:

$$\gamma_k = Z_k \Gamma \tag{16}$$

where Γ is the total surface site density in moles per unit surface defined as a physical property of the surface phase.

The evolution equation for γ_k is:

$$\frac{\mathrm{d}\gamma_k}{\mathrm{d}t} = \frac{\sigma_k \dot{s}_k}{W_k} \tag{17}$$

with σ_k, the number of surface sites occupied by a molecule of the k^{th} species; $\dot{s}_k$, the net rate of k^{th} species production by the heterogeneous reactions.

The initial state of the surface is defined by imposing surface site fractions Z_{k0}; the surface temperature is supposed to be equal to the particle temperature T_{p0}. With the steady-state assumption, the surface species are considered at equilibrium state, which implies $\dot{s}_k = 0$; in this case, equations (17) can be integrated in pseudo-time until the surface site densities are fully established.

The surface kinetics allows calculating the rates of production of the bulk and gas species per unit surface area. The rates of production of the bulk species $\dot{s}_k$, $k \in [k_B, K_B]$ are used in equations (4) and (5) of the particle model. The rates of production of the gas species $\dot{s}_k$, $k \in [k_G, K_G]$ are needed for the interface conditions with the gas flow, which are formulated as balance equations for the mass and energy fluxes. The mass flux balance equation for the k^{th} gas species is:

$$\rho\, u\, Y_k + J_k = \dot{s}_k, \qquad k \in [k_G, K_G] \tag{18}$$

where the left-hand side represents the sum of mass fluxes by convection and diffusion on the gas side. The convection velocity u, called the Stefan velocity is defined by:

$$u = -\frac{1}{\rho} \sum_{k=k_G}^{K_G} \dot{s}_k \tag{19}$$

The mass fractions of the gaseous species on the droplet surface can be found by solving the system of equations (18).

The heat flux absorbed by the droplet is:

$$q_{alu} = -\left(q_{gas} + \sum_{k=1}^{K_{tot}} h_k\, \dot{s}_k \right) \tag{20}$$

On the right-hand side, q_{gas} is the heat flux in the gas phase including the Fourier and Dufour terms from (15); the second term is the thermal effect of all the heterogeneous reactions. K_{tot} is the total number of species in the three phases. For the particle model including a cap, it is supposed the heat exchange by conduction is effective on the whole surface area A_p whereas the heat exchange due to the convection and diffusion takes place on the droplet surface only. The heat rate absorbed by the particle is finally expressed as:

$$Q_p = A_p (\lambda \nabla T)_{gas} - A_{alu} \left(\sum_{k=k_G}^{K_G} P \chi_k v_k + \sum_{k=1}^{K_{tot}} h_k\, \dot{s}_k \right) \tag{21}$$

The gas temperature at the particle surface is equal to the particle temperature T_p. With the steady-state assumption, T_p is found by solving (21) under adiabatic condition $Q_p = 0$ excepting the boiling regime, for which $T_p = T_b$.

2.5 Conditions for the gas flow on the outer boundary

Two types of boundary conditions are considered in the present study: (i) open boundary with fixed temperature and composition for the oxidizer; (ii) closed boundary with zero mass and energy fluxes.

The 1st type can be used with the unsteady or steady-state approach. These conditions are artificial being applied to a 1D steady flow but their influence is pronounced in a limited zone near the boundary. There is no influence on the flow zone between the particle and the flame if the outer boundary is set sufficiently far from the particle surface. As a benefit, it is possible to take into account the effect of oxidizer convection by adjusting the position of the outer boundary, which is proved by 1D simulations in comparison with 2D simulations.

The 2nd type can be used with the unsteady approach only. In this case, the mass and energy of the system (particle plus oxidizer) are conserved. Gas heating during the combustion process results in gas

DOI: 10.13009/EUCASS2019-202

expansion, which is allowed by moving the closed boundary in order to keep the pressure constant. These conditions are useful in a case of oxidizer limitation, which is typical for the solid propellant combustion or for a cloud of particles.

2.5 Solution procedure

For the time-dependent solution, each system of differential equations corresponding to the particle, gas flow and surface models are integrated on a time step by dedicated numerical procedures based on implicit methods for better stability. The time step is controlled by the CFL condition for precise simulation of the flow evolution. On each time step, the droplet state is first updated then the solution for the flow and surface states is advanced in a coupled manner and finally the droplet state is recalculated using the new flow and surface states.

For the gas flow, transport equations (8)-(10) are discretized in a conservative form with the finite volume method. The convective fluxes can be approximated either by the 1st order upwind scheme or a hybrid scheme with variable upwinding depending on the local Peclet number. The molecular transport fluxes are approximated using the standard 2nd order central differencing. With these schemes, the finite difference equations are formulated for a 3-point numerical stencil. The discretized transport equations represent a system of coupled nonlinear equations, which is solved by the Newton-Raphson method. The Jacobian matrix of the system is evaluated numerically. With the steady-state assumption, the gas flow equations can be also integrated in pseudo-time to obtain a nearly-converged solution, which is used as a starting state for solving the system without temporal terms.

Solution errors due to spatial discretization of the gas flow equations are minimized by grid adaptation. With the steady-state assumption, grid adaptation is performed a posteriori by controlling solution variation between grid nodes; solution and grid refinement cycles are repeated until all the grid is well refined in zones of important gradient and curvature of the solution variables. During unsteady simulation, the grid is continuously changing due to the particle regression and possible expansion of the flow domain so the a posteriori refinement is not a useful technique. The grid is usually adapted for the initial state then the grid nodes are redistributed at each time step between the mowing boundaries; the grid steps change proportionally to the radial coordinate in log scale so that the grid near the particle is less affected by the domain dilatation.

3. Validation of the modeling approach

The purpose is validate the new 1D modeling approach as well as the surface kinetic mechanism being applied to a problem of aluminum combustion in a solid propellant environment. To our best knowledge, the surface kinetic mechanism of Glorian et al. has not been yet validated in such a complex environment. Three reaction subsets from the original mechanism [5] are tested: aluminum evaporation and aluminum oxides reactions (Al-O), Al-O subset extended with the hydrogenated species reactions (Al-O-H), and Al-O-H subset extended with the carbonated species reactions Al-O-H-C. The heterogeneous reactions for species containing N and Cl atoms, available in the original mechanism, are not used in this study; the reason is that they result in a quick blockage of the droplet surface by adsorbed species, which are not properly eliminated.

Two validation cases are presented below. The first one is to compare 1D quasi-steady modeling results with experimental data. The second presents a comparison between 1D and 2D simulations.

The experimental case of Chen et al. [11] is first used to validate the 1D modeling approach. A 300 μm droplet is burning in a solid propellant environment. The oxidizer composition is defined in the Table 1. The ambient pressure is 83 kPa and the temperature is 2537 K. The particle is modeled without cap. The outer boundary of the gas flow is set at a distance $r/r_p = 1000$.

Table 1 – Oxidizer composition in mole fractions corresponding to the experiment by Chen et al. [11].

Cl	CO	CO_2	H	H_2	H_2O	HCl	HO	N_2	NO	O	O_2
0.0136	0.1418	0.1037	0.0094	0.0822	0.3751	0.1703	0.0094	0.0917	0.0007	0.0007	0.0013

Simulated radial profiles of temperature are compared with the experimental and modeling results by Chen et al. [11] in Figure 2. The modeling results by Chen et al. lie within the experimental scatter but seem to be higher than their average level. The present results obtained with the Al-O surface mechanism (green line) show the best agreement with the averaged measurement data. With both Al-O-H and Al-O-H-C surface

DOI: 10.13009/EUCASS2019-202

mechanisms, the temperature in the flame is considerably overestimated. It is found by analyzing the thermal effect of the heterogeneous reactions that those involving hydrogen and carbon containing species produce a strong exothermic net effect, which results in the observed increase of temperature on the particle surface and in the flame.

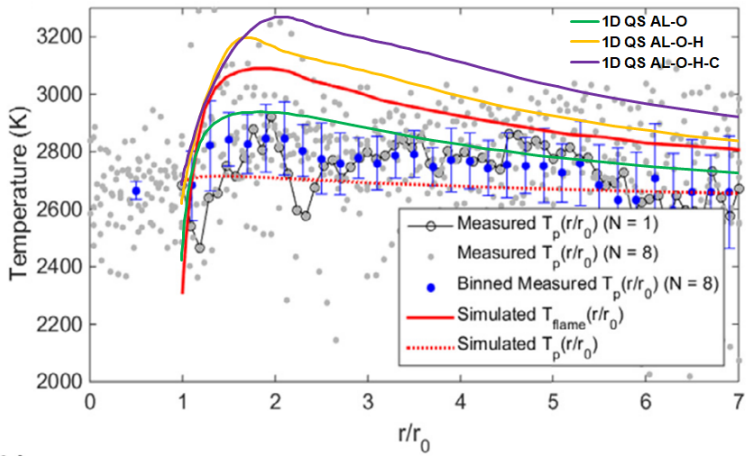

Figure 2 – Comparison of the temperature profiles from the 1D quasi-steady (QS) simulations with the experimental (points) and modeling (red lines) results by Chen et al.

The second validation case is a comparison between 1D and 2D numerical results with the quasi-steady-state assumption. The same thermochemical and molecular transport models are used for both approaches. The surface chemistry is represented by the Al-O mechanism. A 132 µm droplet burns under conditions typical for the Ariane 5 solid booster with a pressure of 5 MPa and an oxidizer temperature of 2330 K. The oxidizer composition is defined in the Table 2. No cap is considered in both cases.

Table 2 – Oxidizer composition in mole fractions for the solid booster case.

H_2	HO	H_2O	Cl	HCl	CO_2	CO	N_2
0.0127	0.0002	0.2499	0.0007	0.2566	0.1444	0.2352	0.1002

In the 2D simulation, the outer boundary is concentric with the droplet and situated at a distance of 100 r_p; the oxidizer conditions are imposed together with an axial velocity of 1.7 m/s on the left half of the boundary. A structured computational mesh is composed of radial lines, uniformly distributed, and circular lines, whose radial distribution corresponds to the adapted grid in the 1D simulation.

Flowfield around the particle is strongly affected by the oxidizer convection in the 2D simulation. This can be seen in Figure 3 presenting the fields of temperature and $Al_2O_3(L)$ mass fraction together with streamtraces in the vicinity of the droplet. As the convection effect is important, both fields show strong differences between the upwind and downwind sides. The flame temperature is significantly higher and the flame zone is much thicker behind the particle. The qualitative difference is even more pronounced for the $Al_2O_3(L)$ species.

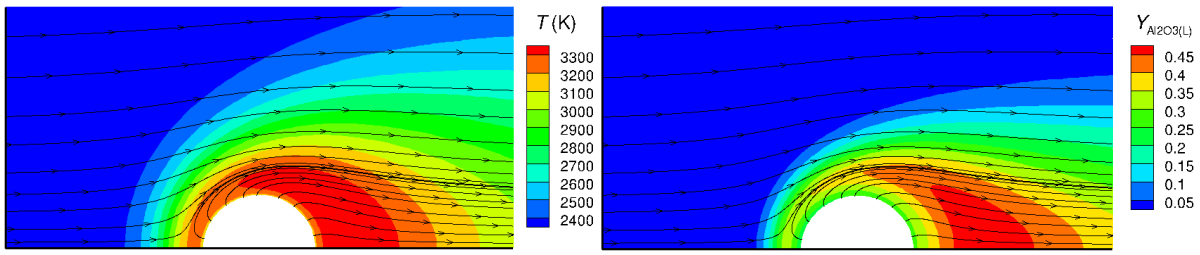

Figure 3 – 2D flowfield in the vicinity of a burning aluminum particle: temperature on the left and $Al_2O_3(L)$ mass fraction on the right with superimposed streamlines.
Only the upper half of the axisymmetric field is shown.

To take into account the convection effect in the 1D simulation, the distance to the outer boundary has

DOI: 10.13009/EUCASS2019-202

to be adjusted so that the mass flow rate at the droplet surface obtained in the two simulations is the same. As the convection effect is strong, the outer boundary is set at a distance of only 2.07 r_p.

Figure 4 shows radial profiles of temperature and Al mass fraction from the 1D and 2D simulations. The 2D simulation is represented by three profiles extracted from the flowfield along different directions: upwind, transverse (normal to the axis), and downwind. One can notice that the 1D profiles are in good agreement with the 2D upwind profiles but not with the transverse and downwind ones which have significantly higher levels for both quantities. This comparison indicates that the conditions on the windward side are determinant for the overall burning rate. Globally, the 1D profiles follow well the trend of the 2D upwind profiles for the species produced at the droplet surface or next to it (Al, AlCl, Al_2O). For the species coming from the oxidizer side of the flame, the agreement in not as good due to the convection effect.

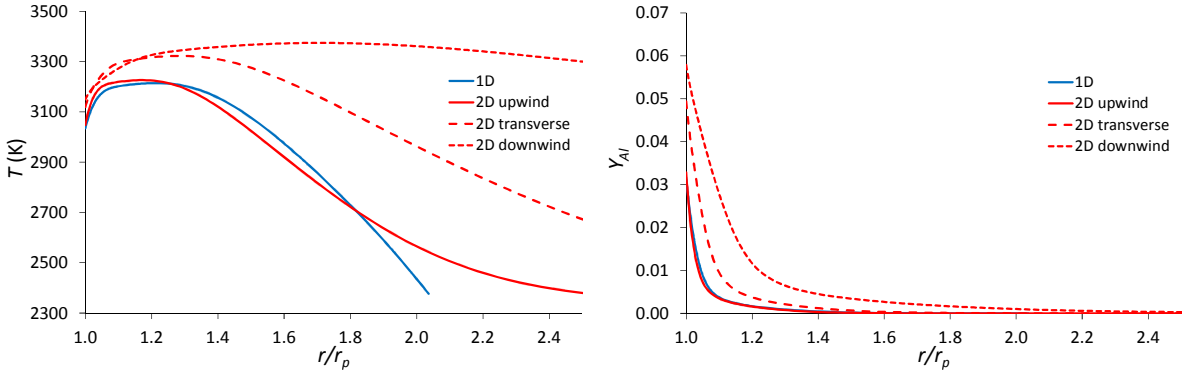

Figure 4 – Comparison of 1D and 2D simulation results: radial profiles versus normalized radial distance for temperature on the left and Al mass fraction on the right.

In the Table 3, the particle surface conditions, obtained in the 1D and 2D simulations, are presented in terms of temperature, mass flux of Al(B) consumption, and site fractions of the main surface species. For the 2D simulation, the upwind, downwind and mean values are given. In 2D, the overall variation with respect to the mean level is from –68 to +39 K for the particle temperature and +43 to 59 % for the mass flux. In this case, the droplet consumption is more promoted by the oxidizer transport towards the surface than by its temperature. Interesting that in the 1D simulation, the particle temperature is close to the 2D upwind value. The species site fractions vary as well over the particle surface however the major species $Al_2O(S)$ remains at almost constant level in the 2D simulation. The 1D results agree well for $Al_2O(S)$ and are within the variation range for the other surface species.

Table 3 – Particle surface conditions from the 1D and 2D simulations:
temperature, mass flux of Al(B) consumption and site fractions of main species.

Data source	T_p (K)	Mass flux ($kg/m^2/s$)	Al(L)	$Al_2O(S)$	$Al_2O_2(S)$	O(S)
1D	3035	2.140	0.1773	0.8076	0.0145	0.0006
2D upwind	3040	3.071	0.1697	0.7948	0.0348	0.0007
2D mean	3108	2.137	0.1959	0.7961	0.0075	0.0005
2D downwind	3147	1.267	0.2149	0.7829	0.0018	0.0005

4. Unsteady simulations of aluminum particle combustion

Previously presented results were obtained with the quasi-steady-state assumption, which correspond to some fixed states of the particle and the surrounding gas. With 1D unsteady approach, it is possible to simulate the whole combustion process both for the particle and the oxidizer. The results presented in this part demonstrate this capability. The main purpose is to study the effect of surface reaction mechanism on the combustion process and its integral characteristics like burning time and residue size.

Four reaction subsets of the surface kinetic mechanism [5] are used in this study: aluminum evaporation

DOI: 10.13009/EUCASS2019-202

reaction only and three previously introduced subsets (Al-O, Al-O-H, and Al-O-H-C). With evaporation only, the particle is composed uniquely of Al(B) as single component droplet (SCD). With the other surface mechanisms, the formation of the cap during the combustion is modeled, so the particle is multi-component (MCD). The cap can be composed of Al_2O_3(B), H(B), and Al_4C_3(B). The last two species are formed by the Al-O-H and Al-O-H-C mechanisms as products of global irreversible reactions eliminating surface species H(S) and C(S). The resulting effect may be unphysical because H(B) are Al_4C_3(B) simply included in the cap mass; they have different thermodynamic properties but their density is supposed to be the same as for Al_2O_3(B).

The oxidizer conditions are the same as for the previous validation case typical for the Ariane 5 solid buster. Two initial particle sizes are considered representing different particle classes: “primary particle” with D_0 = 34 µm and “agglomerate” with D_0 = 120 µm. It is assumed that the initial particle temperature is the same as the oxidizer temperature ($T_{p,0}$ = 2330 K). The gas flow domain has closed outer boundary and its volume is defined by the initial mass proportion of 18 % Al(B) and 82 % oxidizer. The initial oxidizer composition is at equilibrium.

For the surface species, two assumptions were tested regarding their initial fractions: (i) 100 % of Al(L) and (ii) equilibrium composition. The numerical tests show that the two cases differ only in terms of the surface composition during a short initial time period t < 0.2 ms. No effect is observed on the evolution of the main particle parameters. All the 1D simulation results presented below were obtained with the first assumption.

Temporal evolutions of the particle diameter D_p and temperature T_p obtained in the 1D simulations are shown in Figure 5 and Figure 6 respectively. Globally, common trends are observed for the profiles corresponding to the agglomerate and primary particle. In all the cases, the combustion follows three stages. First, the particle is heated up and starts burning, so its temperature increases more or less quickly depending on the surface reaction mechanism; the particle diameter can decrease slowly or remain almost constant or even increase due to the particle thermal expansion. Second, the combustion establishes with a more or less stable particle temperature and a faster decrease of diameter. Third, a quick variation of particle temperature can be observed during a short final stage.

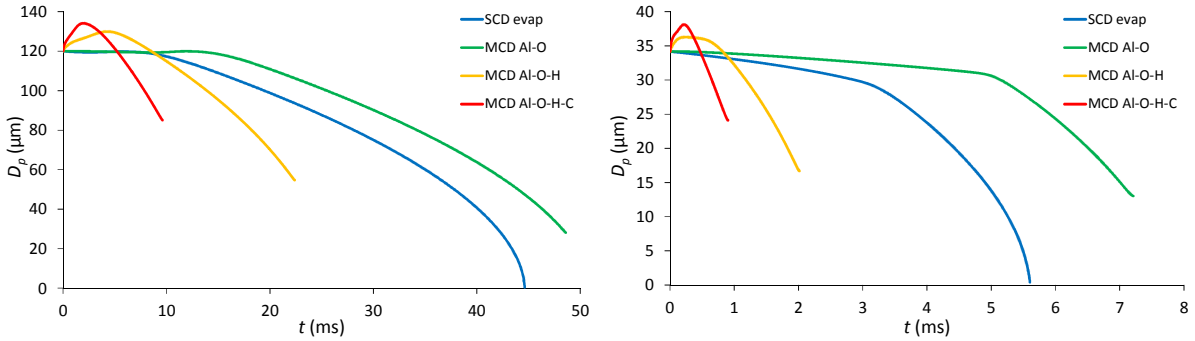

Figure 5 – Temporal evolution of particle diameter for the agglomerate (on the left) and primary particle (on the right) with different surface mechanisms.

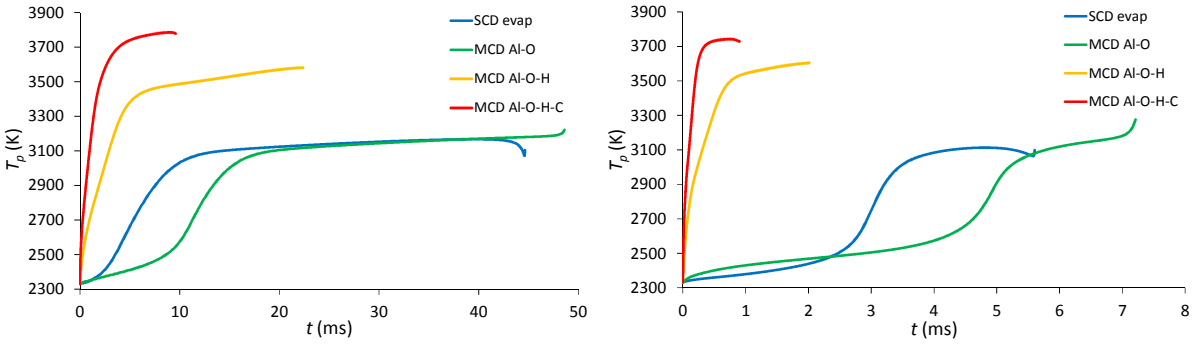

Figure 6 – Temporal evolution of particle temperature for the agglomerate (on the left) and primary particle (on the right) with different surface mechanisms.

Consider the 1st combustion stage with the Al evaporation only (SCD case), which lasts about 10 ms for the agglomerate and more than 3 ms for the primary particle, quite a long period with respect to the burning time. D_p remains almost constant for the agglomerate or decreases slowly for the primary particle because the

DOI: 10.13009/EUCASS2019-202

mass loss by evaporation is compensated by thermal expansion of the particle. T_p starts rising slowly without flame then grows faster during the flame development until T_p becomes close to 3100 K. For the agglomerate, the slow phase of temperature rise is relatively short but the overall heating time is important due to the particle thermal capacity; on the contrary, the heating time of the primary particle is mainly defined by the slow phase duration.

With the Al-O surface mechanism, the 1st combustion stage is longer by about 5 and 2 ms for the agglomerate and primary particle respectively because the slow phase of temperature rise becomes much longer especially for the agglomerate; the further parameter evolution is similar to the SCD case. This behavior is linked to the ignition and flame development processes, which depend on the evaporation rate. The latter can be limited by the surface fraction of Al(L) if it is strongly reduced in presence of the other surface species. This effect can be seen from the surface species profiles for the agglomerate as shown in Figure 7. The fraction of Al(L) falls almost instantly from 100 % to less than 10 % and remains at this level during first 10 ms while Al_2O_2(S) dominates on the particle surface. When the surface temperature becomes high enough, Al_2O_2(S) reduces in favor of Al_2O(S) and Al(L) so the evaporation rate increases and the flame development accelerates with a positive backfeed to the particle heating. The transition process terminates at $t \approx 15$ ms then the main site fractions stay almost constant up to the end of combustion. Qualitatively similar observations can be made of the primary particle.

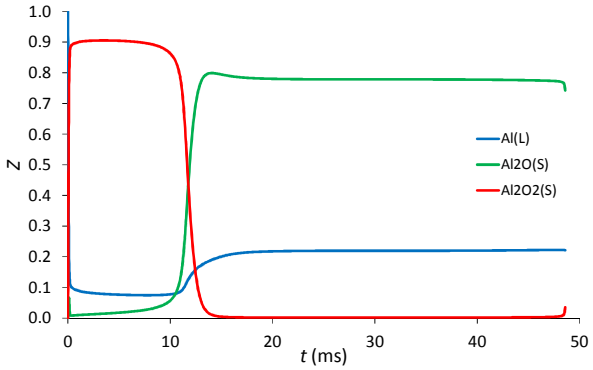

Figure 7 – Site fractions of the main surface species versus time for the agglomerate with the Al-O surface mechanism.

The 2nd stage of established combustion is similar for the Al evaporation only (SCD case) and Al-O mechanism in terms of parameter evolution and duration. During the 3rd final stage, T_p demonstrates different trends (see Figure 6). The negative trend in the SCD case can be due to increasing role of the endothermic effect from evaporation with respect to the heating from the degenerating flame on a small particle. The positive trend in the MSD Al-O case is because the particle receives more heat from the surrounding hot gas through the cap surface. Considering the green plots in Figure 5, one can notice that the residue size D_r related to the initial size D_0 is smaller for the agglomerate than for the primary particle.

The use of the Al-O-H and Al-O-H-C surface mechanisms produces strongly different results for the particle diameter and temperature with respect to those discussed above. During the 1st stage, particle heating is fast from the very beginning and much more intense so D_p increases due to thermal expansion. The combustion process establishes within 3 to 6 ms for the agglomerate and less than 1 ms for the primary particle. The 2nd stage of established combustion is also short with a gradual increase of T_p. The burning time is short because the particle burns at much higher T_p than in the cases considered above: approximately by 400 K with Al-O-H and 600 K with Al-O-H-C. The observed differences in the T_p evolution are due to the thermal effect of heterogeneous reactions involving hydrogen and carbon containing species. To take a closer look, the heat rates provided by these reactions and the Al evaporation reaction are given in Table 4 for time instants corresponding to the 1st stage. Main endothermic effect on the order of 29 MW/m^2 is produced by the Al evaporation reaction for both surface mechanisms; the global reaction of O(S) elimination has much smaller endothermic effect. The other surface reactions provide exothermic effects. The most important one is from the H adsorption reaction, almost compensating the endothermic effect of Al evaporation. The total effect of the three reactions with the AlH(S) species is of comparable value. Already the reactions with hydrogen containing species in both surface mechanisms provide an exothermic net effect from 16 to 19 MW/m^2. In addition, the CO(S) dissociation reaction

DOI: 10.13009/EUCASS2019-202

in the Al-O-H-C mechanism is strongly exothermic and together with the two remaining reactions adds about 15 MW/m^2.

Table 4 – Heat rates of heterogeneous reactions in the Al-O-H and Al-O-H-C mechanisms for the agglomerate.

Surface mechanism	Al-O-H	Al-O-H-C
Time instant, t (ms)	4	1
Reactions	**Heat rate (MW/m^2)**	
Al+Al(L) ⇔ Al(B)+Al(L)	28.8	29.7
3O(S)+2Al(L)+5Al(B) ⇒ Al_2O_3(B)+5Al(L)	≈ 0	1.1
H+Al(L) ⇔ H(S)+Al(B)	–23.8	–27.1
Al(L)+H ⇔ AlH(S)	–8.2	–9.5
AlH(S)+Al(L) ⇔ Al(L)+H(S)+Al(B)	–6.5	–7.1
AlH+Al(L) ⇔ AlH(S)+Al(B)	–6.5	–6.2
$\Sigma_{Al\text{-}O\text{-}H}$	**–16.2**	**–19.1**
CO(S) ⇔ C(S)+O(S)	–	–11.5
3C(S)+4Al(L)+7Al(B) ⇒ Al_4C_3(B)+7Al(L)	–	–2.8
CO+2Al(L) ⇔ CO(S)+2Al(B)	–	–0.6
$\Sigma_{Al\text{-}O\text{-}C}$	–	**–14.9**

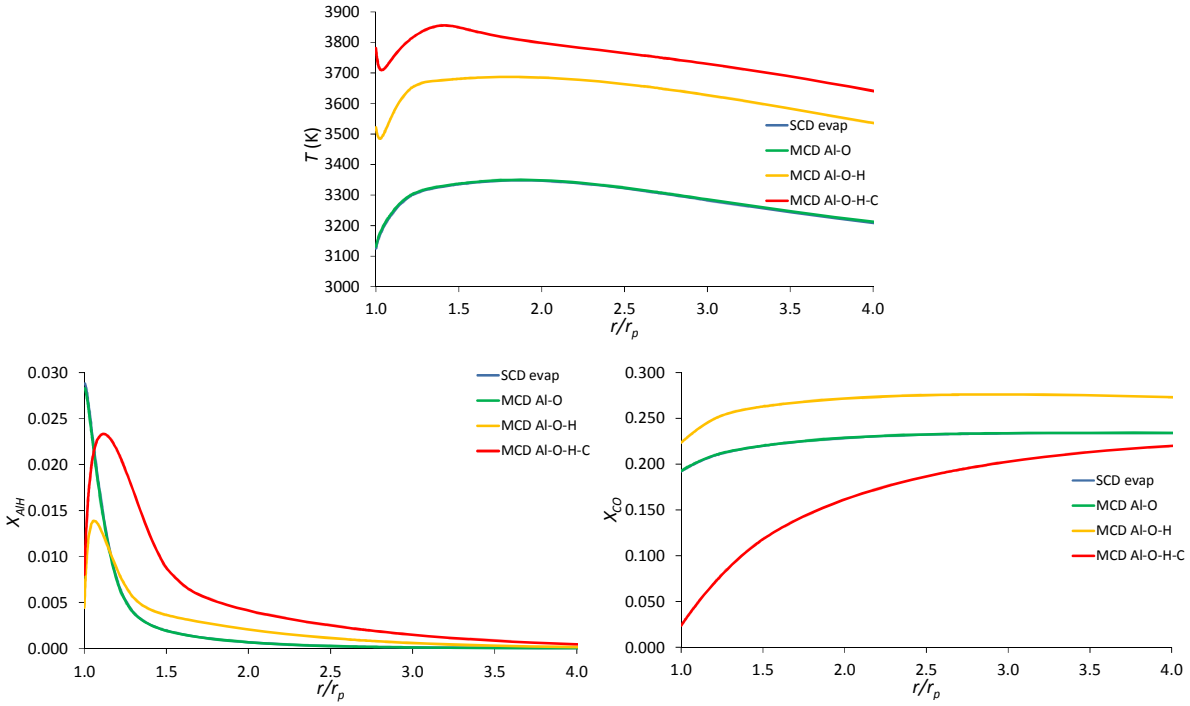

Figure 8 – Radial profiles of temperature (on the top), AlH and CO mole fraction (on the bottom left and right) in the flame zone for the agglomerate at the time instant when $D_p \approx 100$ µm.

The strong effect of the surface reaction mechanism on the flame is illustrated by the radial profiles of gas temperature and of AlH and CO mole fraction, which are shown in Figure 8. The time instant is chosen for each case when the particle size is about 100 µm. The profiles for the Al evaporation only (SCD case) and Al-O mechanism are coincident so at this early moment of established combustion, neither the Al-O surface chemistry nor the cap presence is influencing the flame structure. In these two cases, the temperature profile has a unimodal shape with a maximum at approximately 2 r_p; AlH is generated in the gas phase near the particle surface where it reaches its maximum; CO is transported by diffusion from the oxidizer side and it is weakly reactive so its fraction gradually decreases towards the particle surface. With the Al-O-H and Al-O-H-C surface mechanisms, the net effect of heterogeneous reactions is strongly exothermic and results in overall temperature increase as well as a local maximum at the particle surface; the maximum temperature in the flame is higher by about 350 and 550 K in accordance with the exothermicity of heterogeneous reactions. AlH consumption by the

DOI: 10.13009/EUCASS2019-202

adsorption reactions results in a steep reduction of the AlH fraction near the surface. The profile of CO fraction shows also a strong effect of CO adsorption with the Al-O-H-C mechanism.

Dynamics of the cap growth during the combustion process is shown in Figure 9 by temporal evolutions of the equivalent diameter D_{cap} corresponding to the cap volume. With the Al-O surface mechanism, D_{cap} increases during the 1st combustion stage and then remains nearly constant up to the end of combustion. For example, in the agglomerate simulation, D_{cap} grows up to 26 µm during first 12 ms and only to 27.8 µm at the end of combustion. The cap is composed of Al_2O_3(B), which is mainly formed as a product of the global reaction for O(S) elimination. With the Al-O-H and Al-O-H-C mechanisms, there is no evident relation of the D_{cap} growth with the combustion stages. In both cases, D_{cap} grows rapidly at the very beginning of the 1st combustion stage. Then the growth rate reduces suddenly for Al-O-H and stays low. With Al-O-H-C the growth rate is changing rather gradually all the way.

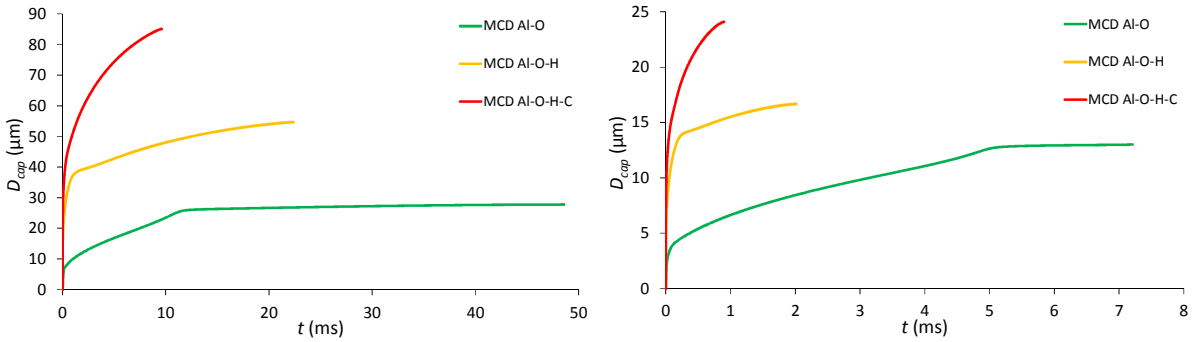

Figure 9 – Equivalent cap diameter versus time for the agglomerate (on the left) and primary particle (on the right) with different surface mechanisms.

More insight in the cap formation process can be gained by considering temporal evolutions of the mass fractions of different bulk constituents of the particle. They are plotted in Figure 10 for the three surface mechanisms. With the Al-O mechanism, the cap is composed solely of Al_2O_3(B) and represents a small fraction of particle mass at the end of the 1st combustion stage: on the order of a percent for the agglomerate and about 10 % for the primary particle. The following evolution of $Y_{Al2O3(B)}$ is defined by consumption of the bulk aluminum Al(B). With the Al-O-H and Al-O-H-C mechanisms, the cap formation process is more complex as it involves more bulk species but in both cases, the initial rapid growth of the cap is due to the short period of Al_2O_3(B) formation; production of H(B) is permanent but much slower. These observations explain the abrupt change in the growth rate of D_{cap} previously discussed in relation with Al-O-H mechanism (see Figure 9). The effect of H(B) generation is however very important with this latter mechanism because the final cap mass is composed of 40% Al_2O_3(B) and 60% H(B) for the agglomerate; the proportions change reciprocally for the primary particle. Al_4C_3(B) is generated faster than H(B) by the Al-O-H-C mechanism providing the high rate of cap growth, as it was shown in Figure 9. Due to the short burning time, the final cap mass contains Al_2O_3(B) and Al_4C_3(B) in nearly equal proportions and less than 10 % of H(B) for both particle classes.

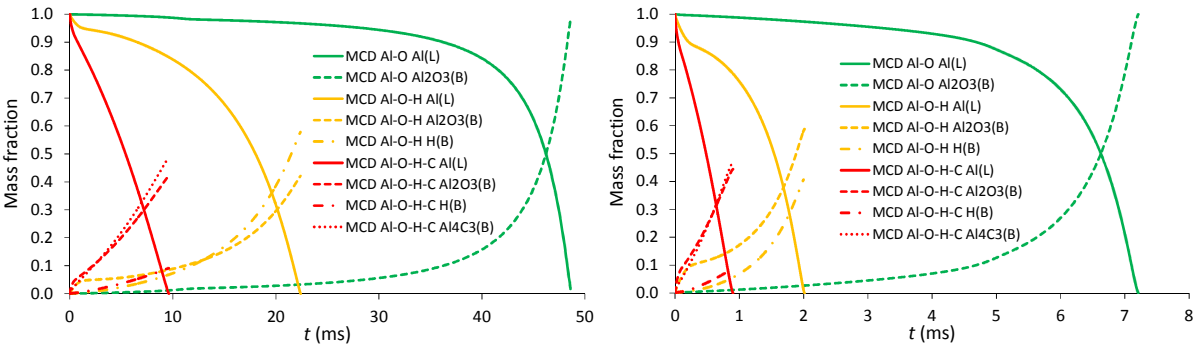

Figure 10 –Mass fraction of the bulk components versus time for the agglomerate (on the left) and primary particle (on the right) with different surface mechanisms.

The burning time τ_b and residue diameter D_r (final value of D_{cap}) are given in Table 5 for all the studied cases. The burning time includes the duration of the three stages discussed above. The largest τ_b for both particle classes is obtained with the Al-O surface mechanism because of the longer 1st stage with respect to the cases

DOI: 10.13009/EUCASS2019-202

with the Al evaporation only. With the other two mechanisms, τ_b is much shorter and demonstrates similar trends for both particle classes. For the cases with cap formation, larger D_r values correspond to shorter τ_b.

Table 5 – Burning time and residue diameter obtained with different surface mechanisms for the two particle classes.

Class	Surface mechanism	τ_b (ms)	D_r (µm)
Agglomerate, D_0 = 120 µm	Al evaporation only	44.6	0
	Al-O	48.6	27.8
	Al-O-H	22.4	54.7
	Al-O-H-C	9.6	85.1
Primary particle, D_0 = 34 µm	Al evaporation only	5.6	0
	Al-O	7.2	13.0
	Al-O-H	2.0	16.7
	Al-O-H-C	0.9	22.1

Using the values of D_0 and τ_b from Table 5, it is possible to estimate the power exponent of the burning time law $\tau_b \sim D_0^n$ corresponding to the four surface mechanisms: 1.65, 1.51, 1.92, and 1.88. The $\tau_b(D_0)$ function shows the smoothest trend with the Al-O mechanism and the steepest with the Al-O-H one. It is however difficult to interpret the relation between the surface mechanisms and the n values because of the high complexity of the modeled processes. Instead, we will try analyzing the temporal variations of the droplet geometry to identify the changes in the combustion regime at particular stages. As a reasonable choice, the droplet size is represented by the equivalent diameter corresponding to the open surface of the aluminum droplet:

$$D_{alu} = \sqrt{A_{alu}/\pi} \tag{22}$$

At a given time instant t, the following function is used to evaluate the local n-exponent:

$$\tau_b - t = a\, D_{alu}(t)^{n_{loc}} + b \tag{23}$$

where a and b are fit coefficients determined for a short interval around t.

The obtained temporal variations of n_{loc} are shown in Figure 11. One should note that there is no correspondence between the global n values given above and the $n_{loc}(t)$ curves because in the latter case the droplet and oxidizer states are constantly changing in time.

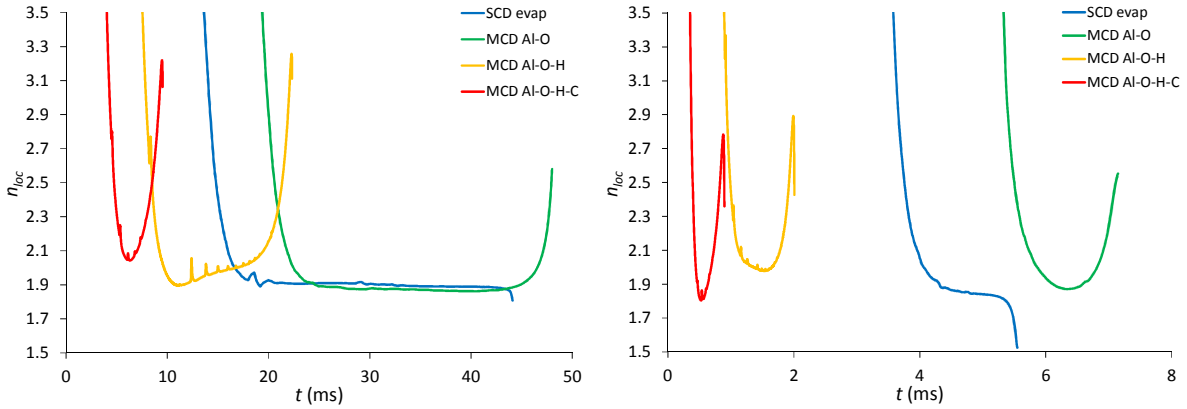

Figure 11 – Temporal evolution of the local D^n law exponent for the agglomerate (no the left) and the primary particle (on the right) with different mechanisms.

During the 1st combustion stage, the particle is strongly affected by thermal expansion and the evolution of n_{loc} is chaotic, so there is no much sense in considering this stage. When the combustion is established, n_{loc} goes down rapidly to a level between 1.8 and 2, which corresponds to the diffusion-controlled regime. The following evolution depends on the surface mechanism. With the Al evaporation only (SCD case), n_{loc} stays for a while near 1.9 then decreases sharply during the final combustion stage for both particle classes. This decrease may be interpreted as a transition towards the kinetically controlled regime. The curves for the Al-O mechanism demonstrate a similar evolution of n_{loc} excepting the final stage, during which n_{loc} rises to 2.5. The observed difference must be due to the cap effect, which is increasing strongly at the end of combustion and is more

DOI: 10.13009/EUCASS2019-202

pronounced for the primary particle as its cap is relatively larger. It has been already mentioned that the cap favors particle heating during the final stage of combustion. With the Al-O-H mechanism, n_{loc} is between 1.9 and 2 in the lowest portion of the curves. With the Al-O-H-C mechanism, the curves are a narrow minimum above 2 for the agglomerate and near 1.8 for the primary particle. With these two mechanisms, the following rise of n_{loc} is above 3.2 for the agglomerate and 2.8 for the primary particle. This strong rise of n_{loc} can be explained by the cap effect, which must increase as a function of the cap size. At the very end of combustion, the curves show a sudden drop of n_{loc}, which may be related to a rapid reduction in the exothermic effect of the surface reactions.

5. Discussion

The new 1D modelling approach used in this study represents a powerful numerical tool to test detailed combustion models and to simulate the aluminum particle combustion under representative conditions of a solid rocket motor. The cap effect is modeled in a simplified manner but allows taking into account the mass and energy budget within the particle as well as the evolution of the reactive droplet surface in connection with the particle geometric model. The assumption concerning instantaneous absorption by the cap of the bulk species produced on the droplet surface may have a strong effect on the integral rate of heterogeneous reactions because insoluble bulk species, like alumina for example, can form films and thus reduce the effective reactive surface. Direct observations of burning aluminum particles [17]-[19] show examples of combustion regimes with irregular flame configurations. The cap surface itself can participate in the mass exchange through deposit of alumina particles from the gas phase as well is in condensed-phase reactions with dissolved species [17][18]. Nevertheless, the current approach is well-suited for parametric analysis and comparative studies with different physico-chemical models.

The simulation results demonstrate strong influence of the surface reaction mechanism on the predicted burning time and the size of the combustion residue. The data for τ_b from Table 5 can be compared with the well-known correlation by Beckstead [20] as shown in the Figure 12. The predictions with the Al evaporation only and Al-O mechanism are higher respectively by factors 1.5 and 1.63 for the agglomerate and by factors 1.80 and 2.32 for the primary particle. This significant discrepancy can be due to the 1st stage, which takes 10 to 15 ms for the agglomerate and 3 to 5 ms for the primary particle. In the unsteady simulations, the influence of the oxidizer convection is not taken into account however it can be a strong factor reducing the time needed for combustion establishment. After subtracting the 1st stage duration from the τ_b values, the results agree much better with Beckstead's correlation. On the contrary, the Al-O-H and Al-O-H-C mechanisms provide significantly lower predictions respectively by factors 0.75 and 0.32 for the agglomerate and by factors 0.65 and 0.29 for the primary particle. Together with the validation results shown in Figure 2, the present analysis suggests that the use of the latter mechanisms with the current modeling approach produces erroneous results. In particular, it could be due to some deficiencies in the surface kinetics because the bulk species are generated by global reactions, whose main role is to eliminate particular surface species.

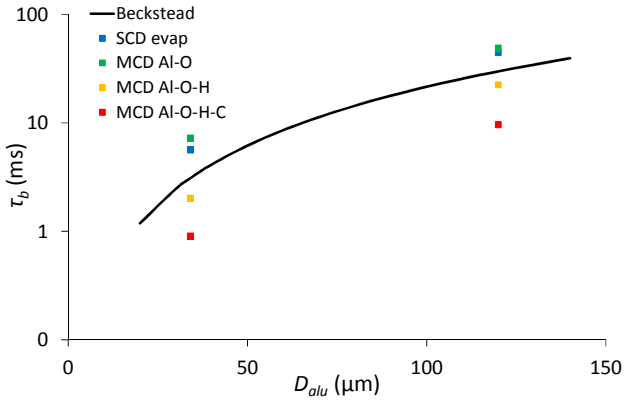

Figure 12 – Combustion time versus equivalent diameter corresponding to the open surface of the aluminum droplet for the four mechanisms and the Beckstead correlation

It is of course not a proof that the hydrogen and carbon containing species should not be considered in the heterogeneous reactions. The experimental studies of Sarou-Kanian et al. [17][18][21] provide evidences of complex interactions like dissolution of different species including hydrogen, formation of bubbles inside the

DOI: 10.13009/EUCASS2019-202

particle and films on its surface, carbon accretion as well as various phase changes. Aluminum carbide and oxicarbide can represent an important fraction of combustion residues [18]. Nitrogen and chlorine containing species need also to be included in the surface kinetics in a proper way because they have significant influence on the combustion time [22][23]. Aluminum nitrate and oxinitrate were found in combustion residues [17].

5. Conclusion

A new 1D combustion model for an aluminum droplet with detailed description of the reaction kinetics and the molecular transport has been developed at ONERA. It has been validated in comparison with the experimental results by Chen et al. [11] providing good agreement for the results obtained with the Al-O surface mechanism. A possibility of taking into account the effect of oxidizer convection by adjusting the outer boundary position has been demonstrated providing good agreement between the 1D and 2D results in a test case representative of the environment in a solid rocket motor.

Using the unsteady approach with a limited quantity of oxidizer, 1D simulations have been carried out with four surface mechanisms, representing different reaction subsets of the kinetic mechanism of Glorian et al. [5], for two particle classes corresponding to an agglomerate and a primary particle. Time histories of several parameters characterizing the particle and its cap have been analyzed in connection with the surface kinetics and the flame. Variations of the combustion regime have been interpreted using local approximations of the burning-time law. It has been found that the surface kinetics has strong influence on the simulation results. In particular, the Al-O-H and Al-O-H-C mechanisms produce an important exothermic effect; as a consequence, the burning time is reduced strongly.

6. Acknowledgments

This work was supported by ONERA and DGA. The authors gratefully acknowledge helpful discussions with Eric Faucher from DGA.

References

[1] Beckstead, M.W., Liang, Y., Pudduppakkam, K.V. 2005. Numerical simulation of single aluminum particle combustion. *Combustion, Explosion and Shock Waves*. 41(6):622–638.

[2] Washburn, E.B., Trivedi, J.N., Catoire, L., Beckstead, M.W. 2008. The simulation of the combustion of micrometer-sized aluminum particles with steam. *Combustion Science and Technology*. 180(8):1502-1517.

[3] Glorian, J. 2014. Cinétique hétérogène pour la combustion de l'aluminium. PhD thesis of ENSTA PariTech.

[4] Glorian, J., Catoire, L., Gallier, S., Cesco, N. 2015. Gas-surface thermochemistry and kinetics for aluminum particle combustion. *Proceedings of the Combustion Institute.* 35(2):2439–2446.

[5] Glorian, J., Gallier, S., Catoire, L. 2016. On the role of heterogeneous reactions in aluminum combustion. *Combustion and Flame*. 168:378-392.

[6] Orlandi, O., Fabignon, Y. 2001. Numerical simulation of the combustion of a single aluminum droplet in various environments. *37th AIAA/ASME/SAE/ASEE Joint Propulsion Conference and Exhibit*. AIAA-2001-3582. Salt Lake City, Utah, USA.

[7] Orlandi, O. 2002. Modélisation et simulation numérique de la combustion d'une goutte isolée d'aluminium. PhD thesis of the University of Orléans.

[8] Cho, S.Y., Yetter, R.A., Dryer, F.L. 1992. A computer model for one-dimensional mass and energy transport in and around chemically reacting particles, including complex gas-phase chemistry, multicomponent molecular diffusion, surface evaporation, and heterogeneous reaction. *Journal of Computational Physics*. 102:160-179.

[9] Bucher, P., Yetter, R.A., Dryer, F.L., Parr, T.P., Hanson-Parr, D.M. 1998. PLIF species and radiometric temperature measurements of aluminum particle combustion in O_2, CO_2 and N_2O oxidizers, and comparison with model calculations. *27th Symposium on Combustion.* The Combustion Institute. 2421-2429.

[10] Savel'ev, A., Starik, M. 2018. The formation of $(Al_2O_3)n$ clusters as a probable mechanism of aluminum oxide nucleation during the combustion of aluminized fuels: Numercial analysis. *Combustion and Flame.* 196:223-236.

[11] Chen, Y., Guildenbecher, D.R., Hoffmeister, K.N.G., Cooper, M.A., Stauffacher, H.L., Oliver, M.S., Washburn, E.B. 2017. Study of aluminum particle combustion in solid propellant plumes using digital in-line holography and imaging pyrometry. *Combustion and Flame*. 182: 225-237.

DOI: 10.13009/EUCASS2019-202

[12] Devillers, R.W., Dorval, N., Vilmart, G., Nugue, M., Le Besnerais, G., Pichillou, J. 2018. Aluminum particle tracking on experimental shadowgraphy and Al-PLIF images to provide velocity data for two-phase flow simulations of solid rocket motors*, Space Propulsion Conference, Sevilla, Spain*.

[13] Vilmart, G., Dorval, N., Attal-Trétout, B., Bresson, A. 2017. Detection of iron and aluminum atomic vapors by LIF technique : application to solid propellant combustion. AIAA 2017-3900, *33rd AIAA Aerodynamic Measurement Technology and Ground Testing Conference*, Denver, Colorado, USA.

[14] Muller, M., Davidenko, D., Giovangigli, V. 2017. Computational study of aluminum droplet combustion in different atmospheres. *7th European Conference for Aeronautics and Space Sciences (EUCASS 2017)*, Milan, Italy.

[15] Ern, A., Giovangigli, V. 1994. Multicomponent Transport Algorithms. *Lectures Notes in Physics*. 24 Springer-Verlag. Berlin.

[16] Ern, A., Giovangigli, V. 1995. Fast and accurate multicomponent transport property evaluation. *Journal of Computational Physics*. 120:105–116.

[17] Sarou-Kanian, V., Rifflet, J.C., Millot, F., Matzen, G., Gökalp., I. 2005. Influence of nitrogen in aluminum droplet combustion. *Proceedings of the Combustion Institute*, 30:2063–2070.

[18] Sarou-Kanian, V., Rifflet, J.C., Millot, F., Gökalp., I. 2006. Aluminum combustion in wet and dry CO_2: Consequences for surface reactions. *Combustion and Flame*, 145(1-2):220-230.

[19] Braconnier, A., Gallier, S., Chauveau, C., Halter, F., 2018. Combustion of single aluminum droplet burning in $O_2/CO_2/N_2$ mixtures, *37th International Symposium on Combustion*, Dublin, Ireland. Work-in-progress poster available at: https://hal.archives-ouvertes.fr/hal-01842345v1/document

[20] Beckstead, M.W. 2004. A summary of aluminum combustion*. RTO/VKI Special Course on Internal Aerodynamics in Solid Rocket Propulsion*. RTO-EN-023.

[21] Sarou-Kanian, V. 2003. Etude expérimentale de la combustion de gouttes d'aluminium en convection forcée : Influence de l'atmosphère gazeuse. PhD thesis of the University of Orléans.

[22] Zenin, A., Kusnezov, G., Kolesnikov, V. 2000. Physics of aluminum particle combustion at convection. AIAA-2000-0849, *38th Aerospace Sciences Meeting & Exibit*, Reno, NV, USA.

[23] Legrand B. 2000. Etude de la combustion de particules d'aluminium et de magnesium : influence de la composition du mélange gazeux et de la pression. PhD thesis of the University of Orléans.